

Closing the Loop: Dynamic State Estimation and Feedback Optimization of Distribution Grids

Miguel Picallo

Saverio Bolognani

Florian Dörfler

Automatic Control Laboratory

ETH Zurich

Zurich, Switzerland

{miguelp,bsaverio,doerfler}@ethz.ch

Abstract—This paper considers the problem of online feedback optimization to solve the AC Optimal Power Flow in distribution grids. This consists in continuously driving the controllable power injections and loads towards the optimal set-points in time-varying conditions and real-time. However, instead of assuming noise-free full state measurement like recent feedback optimization approaches, we connect a Dynamic State Estimation using available measurements, and study its dynamic interaction with the optimization scheme. We certify stability of this interconnection and the convergence of the state estimate and the control inputs towards the true state values and optimal set-points respectively. Additionally, we bound the resulting stochastic error. Finally, we show the effectiveness of the approach on a test case using high resolution consumption data.

Index Terms—Distribution grid state estimation, AC optimal power flow, online feedback optimization, voltage regulation

I. INTRODUCTION

The operation of distribution grids is undergoing a paradigm shift due to the increasing share of controllable elements (generation power, curtailment, reactive power in converters, flexible loads, etc.), and pervasive sensing (smart meters, phasor measurement units, etc.). Moreover, the introduction of communication networks with high resolution sensor sampling, and the fast response offered by the power-electronics interfacing the controllable energy sources, enable to perform control-loop rates at very fast time scales. These new technologies offer the potential advantage of lowering the grid operation cost and promoting more sustainable energy systems. Nonetheless, the unpredictability and the high variability of household loads and renewable energy sources, pose a severe challenge in satisfying the required grid specifications, like voltage levels, thermal limits, etc. Consequently, these specifications need to be enforced through either offline optimization or real-time feedback control.

State-of-the-art optimization methods typically solve an static Optimal Power Flow (OPF) to determine the optimal set-points of these controllable energy sources. However, these

approaches may not succeed in efficiently controlling the system under fast time-varying conditions, since they do not take full advantage of these fast sensor sampling and control-loop rates. On the other hand, the recently proposed online feedback optimization [1], [2], [3], [4], [5] has shown an outstanding performance for real-time power system operation under variable conditions and safety conditions. This online feedback optimization consists in using the grid state measurements as feedback to a controller, that continuously drives the controllable power injections towards the optimal set-points. It has been shown, that this feedback optimization offers the advantages of quickly adapting to time-varying conditions [2] and an improved robustness against model-mismatch [5].

However, so far the analysis of all of these feedback optimization approaches have considered a stylized problem setup by assuming a noise-free deterministic system with either full state measurements available, or controlling only directly measurable states. Yet, state measurements are scarce in distribution grids. These grids require a State Estimation (SE) [6] including heterogeneous measurements and pseudo-measurements to make the system numerically observable [7], [8]. Some approaches have already considered using the SE as input to the OPF problem [9], but it has not yet been proposed to include a SE within the scheme of the online feedback optimization. There is one main obstacle on the way: even if the SE and the feedback optimization are both separately stable, optimal, and converge, this does not guarantee that their interconnection will inherit these properties.

Therefore, in this paper, we combine a dynamic SE Kalman filter and the online feedback optimization. Our contribution relies in formally proving that the interconnection of the grid dynamics, the SE, and the feedback optimization is stable and steady-state optimal. More concretely, we certify that in the presence of process and measurement noise, the state estimate and the power set-points delivered by our method converge in expectation to the true state and the optimal set-points, respectively, and both have a bounded error covariance. Additionally, we show the effectiveness of our approach in the IEEE 123-bus test feeder [10] with highly uncertain pseudo-measurements and high resolution consumption data.

The rest of the paper is structured as follows: Section II

Funding by the Swiss Federal Office of Energy through the project Renewable Management and Real-Time Control Platform (ReMaP) (SI/501810-01) and the ETH Foundation is gratefully acknowledged.

introduces some preliminaries: the distribution grid model, the optimization problem setup and its linearisation, and the measurements available. Section III presents the proposed method combining SE and feedback optimization, and proves its stability and convergence. Finally, in Section IV the approach is validated on a simulated test feeder.

II. PRELIMINARIES

A. Distribution Grid Model

A distribution grid can be modelled as a graph $\mathcal{G} = (\mathcal{V}, \mathcal{E}, \mathcal{W})$ with nodes $\mathcal{V} = \{1, \dots, N_{\text{bus}}\}$ representing the buses, edges $\mathcal{E} = \{(v_i, v_j) \mid v_i, v_j \in \mathcal{V}\}$ representing the branches, and edge weights $\mathcal{W} = \{w_{i,j} \mid (v_i, v_j) \in \mathcal{E}, w_{i,j} \in \mathbb{C}\}$ representing the admittance of a branch, which is determined by the length and type of the line cables.

In 3-phase networks buses may have up to 3 phases, so that the voltage at bus i , with $n_{\phi,i} \leq 3$ phases, is $V_{\text{bus},i} \in \mathbb{C}^{n_{\phi,i}}$ (and the edge weights $w_{i,j} \in \mathbb{C}^{n_{\phi,i} \times n_{\phi,j}}$). The state of the network is then typically represented by the vector bus voltages $V_{\text{bus}} = [V_{\text{src}}^T, V^T]^T \in \mathbb{C}^{N+3}$, where $V_{\text{pcc}} \in \mathbb{C}^3$ denotes the measured voltage at the point of common coupling (PCC) connected to the main grid, and $V \in \mathbb{C}^N$ are the voltages in the non-source buses, where N depends on the number of buses and phases per bus. Moreover, the set of nodes \mathcal{V} can be separated into the PCC bus, the set of controllable power injections \mathcal{C} , and the set of uncontrollable loads \mathcal{L} : $\mathcal{V} = \{\text{PCC}\} \cup \mathcal{C} \cup \mathcal{L}$.

The Laplacian matrix $Y \in \mathbb{C}^{(N+3) \times (N+3)}$ of the weighted graph \mathcal{G} , also called admittance matrix [6], can be used to express the power flow equations required to compute the currents I and the power S injection at each node:

$$\begin{aligned} \begin{bmatrix} I_{\text{pcc}} \\ I \end{bmatrix} &= Y \begin{bmatrix} V_{\text{pcc}} \\ V \end{bmatrix} = \begin{bmatrix} Y_{00} & Y_{01} \\ Y_{01}^T & Y_{11} \end{bmatrix} \begin{bmatrix} V_{\text{pcc}} \\ V \end{bmatrix} \\ S &= P + jQ = \text{diag}(V) \bar{I} = \text{diag}(V) \left(\bar{Y}_{11} \begin{bmatrix} \bar{V}_{\text{pcc}} \\ \bar{V} \end{bmatrix} \right) \\ \begin{bmatrix} P \\ Q \end{bmatrix} &= \mathbb{I}_c S_c + \mathbb{I}_l S_l \end{aligned} \quad (1)$$

where j is the imaginary unit, $\bar{(\cdot)}$ denotes the complex conjugate, and $\text{diag}(\cdot)$ represents the diagonal operator, converting a vector into a diagonal matrix. The vectors $P, Q \in \mathbb{R}^N$ are the active and reactive powers; $S_c = [P_c^T, Q_c^T]^T \in \mathbb{R}^{2n_c}$, $S_l = [P_l^T, Q_l^T]^T \in \mathbb{R}^{2n_l}$ are the vectors of controllable injections and uncontrollable loads respectively; and $\mathbb{I}_c, \mathbb{I}_l$ are matrices filled with 0, 1 that map the elements of S_c, S_l in the sets \mathcal{C}, \mathcal{L} to the corresponding nodes indices of (P, Q) .

B. Problem Setup

The operation of these distribution grids consists in optimizing the use of the controllable resources while satisfying some grid restrictions. This optimization problem can be represented as a particular case of the AC Optimal Power Flow (AC-OPF):

$$\min_{S_c \in \mathcal{F}, V} f(S_c) + g(V) \text{ s.t. (1)} \quad (2)$$

where

\mathcal{F} : The feasible set \mathcal{F} contains the limits of available power, for example $\mathcal{F} = \{S_c \mid P_{i,\min} \leq P_{c,i} \leq P_{i,\max}, Q_{i,\min} \leq Q_{c,i} \leq Q_{i,\max} \forall i\}$. These are hard constraints to be satisfied all the time.

$f(S_c)$: The objective function $f(S_c) = \sum_{i=0}^{n_c} f_i(S_{c,i})$ determines the cost of the grid operations by adding the costs f_i of using each controllable power i of the total number of n_c controllable elements.

$g(V)$: The objective function $g(V)$ encodes the grid restrictions through the specification of desired states and objectives. These can include power losses, voltage constraints, overload of lines and transformers, etc. More concretely, we will use $g(V) = \frac{\rho}{2} \sum_i^n (\max(0, |V|_i - V_{\max}))^2 + (\max(0, V_{\min} - |V|_i))^2$ to penalize violations of the voltage limits. These are soft constraints that can be violated at a given cost. Actually, they can be transiently violated during the real operation. However, for a large ρ , these restrictions are more likely to be satisfied in steady-state.

C. Power Flow Linear Approximation

The non-linearity of the power flow equations (1) is difficult to handle when solving the optimization problem (2). Actually, for multi-phase unbalanced distribution grid, these equations (1) are generally nonconvex [11]. Hence, linear approximations [12] are used frequently in the literature [2], [5]. Considering the flat voltage (zero injection profile) $V_0 = Y_{11}^{-1} \text{diag}(\bar{V}) - 1$ as operating point, for a polar representation of the state V : $[|V|^T, \angle V^T]^T$, we have the linearisation

$$\begin{bmatrix} |V| \\ \angle V \end{bmatrix} = \begin{bmatrix} |V_0| \\ \angle V_0 \end{bmatrix} + B_c S_c + B_l S_l \quad (3)$$

where, defining $Z_V = Y_{11}^{-1} \text{diag}(\bar{V}_0)^{-1}$, we have

$$B_c = B \mathbb{I}_c, B_l = B \mathbb{I}_l \\ B = \begin{bmatrix} \cos(\angle V_0) & \sin(\angle V_0) \\ -\frac{\sin(\angle V_0)}{|V_0|} & \frac{\cos(\angle V_0)}{|V_0|} \end{bmatrix} \begin{bmatrix} \Re\{Z_V\} & \Im\{Z_V\} \\ \Im\{Z_V\} & -\Re\{Z_V\} \end{bmatrix}$$

where $\Re\{\cdot\}, \Im\{\cdot\}$ denote the real and imaginary part of a complex number.

Instead of the problem (2), we consider then its linear approximation:

$$\min_{S_c \in \mathcal{F}, V} f(S_c) + g(V) \text{ s.t. (3)} \quad (4)$$

D. Measurements

If the current grid state V or the loads S_l are not known, the problem (4) cannot be solved. As a result, we need measurements to estimate these parameters and solve (4).

In distribution grids, there may be a set of heterogeneous noisy measurements, like voltage, current and power magnitudes and/or phasors. However, due to the scarce number of measurements, they may need to be complemented with the so-called pseudo-measurements [7], [8], i.e., low accuracy load forecasts, to make the system numerically observable [13], and thus be able to solve a SE problem. For simplicity, in this paper we will assume that we have a linearised measurement

equation that contains the measurements coming from all sources like conventional remote terminal units, smart meters, phasor measurements units, pseudo-measurements, etc.:

$$y = HV + \omega_y \quad (5)$$

where y is the vector of measurements, H is the matrix mapping the state to the measurements, and ω_y is the measurement noise assumed to be Gaussian with known probability distribution $\omega_y \sim \mathcal{N}(0, \Sigma_y)$. We assume that using the pseudo-measurements, the matrix H has full-column rank, and thus the system is numerically observable [13]. In case of nonlinear measurements, these can be linearised and included in the same equation [8].

Since these pseudo-measurements can be simply load profiles for different kinds of nominal consumption (household, office building, etc.), and thus have a low accuracy, we will assign relatively large values to the corresponding covariance terms in Σ_y indicating a large uncertainty [8]. This large covariance will also lower the effect of a potential bias term in the error noise.

E. Online Feedback Optimization

The online feedback optimization consists of using the actual grid state V as feedback to a controller that drives the controllable power towards the optimal set-points in real-time. Typically, these controllers use a variation of projected gradient descent [4], [5]. The gradient brings the set-points closer to the optimal ones, while the projection forces the solution to remain within the feasible set \mathcal{F} . At every time-step from (t) to $(t+1)$ we update

$$S_{c,(t+1)} = \Pi_{\mathcal{F}}[S_{c,(t)} - \epsilon(\nabla_{S_c} f(S_{c,(t)}) + B_c^T \nabla_V g(V_{(t)}))] \quad (6)$$

where ϵ is the descent rate of the gradient method, $\nabla_{S_c} f(S_c)$ and $\nabla_V g(V)$ are the gradients of f and g respectively, and $\Pi_{\mathcal{F}}[\cdot]$ denotes the projection on the feasible set \mathcal{F} . This expression is derived by computing the gradient of the objective function $f(S_c) + g(V)$ with respect to the decision variables S_c : $\nabla_{S_c}(f(S_c) + g(V)) = \nabla_{S_c} f(S_c) + (\frac{\partial V}{\partial S_c})^T \nabla_V g(V)$, where $\frac{\partial V}{\partial S_c} = B_c$.

Remark 1: Note that in (6) we are assuming that the feasible set \mathcal{F} from (2) and (4) remains constant and independent of time. In a real-world application, it would be time-varying, since the amount of power available may change over time, for example if delivered by renewable sources. However, when considering fast time scales, the change of \mathcal{F} at subsequent instants tends to 0 and can be neglected. We will observe this later in the test case in Section IV. In any case, this work could be extended to a time-varying feasible set $\mathcal{F}_{(t)}$.

III. STATE ESTIMATION FOR FEEDBACK OPTIMIZATION

Apart from the control inputs S_c , which are obviously measurable, the state-of-the-art online feedback optimization approaches such as (6) assume a noise-free deterministic knowledge of the full state V to evaluate $\nabla_V g(V_{(t)})$ [1], [4]. Other approaches restrict g to control only the subset of

directly measured states, so that the states objective function $g(V)$ can be expressed as a function of y [2], [5].

In our approach we consider a more general and realistic scenario, where the whole state V needs to be controlled, but neither the loads S_l nor the state V are measured. To retrieve this information, we use the available measurements y from (5) to build a dynamic SE. Then, we connect this SE as feedback to the controller of the online feedback optimization, instead of using the full state information V as in (6).

A. Dynamic State Estimation

As first step to build this dynamic SE, we subtract the power flow equations (3) at subsequent times (t) to obtain the stochastic dynamic system of the grid state V :

$$V_{(t)} = V_{(t-1)} + B_c(S_{c,(t)} - S_{c,(t-1)}) + \omega_{l,(t)} \quad (7)$$

where $\omega_{l,(t)} = B_l(S_{l,(t)} - S_{l,(t-1)})$ appears as a result of the time-varying load conditions $S_{l,(t)}$. This dynamic approach (7) allows to circumvent the lack of precise knowledge of $S_{l,(t)}$ by considering only its time variations as process noise: $\omega_{l,(t)} \sim \mathcal{N}(0, \Sigma_l)$.

Using (7), we design a Kalman filter based SE [14], that at time (t) takes the measurements $y_{(t)}$ as input and outputs the estimate $\hat{V}_{(t)}$:

$$\begin{aligned} \hat{V}_{(t)} &= (I_d - K_{(t)}H)(\hat{V}_{(t-1)} + B_c(S_{c,(t)} - S_{c,(t-1)})) \\ &\quad + K_{(t)}y_{(t)} \\ P_{(t)} &= (I_d - K_{(t)}H)(P_{(t-1)} + \Sigma_l) \\ K_{(t)} &= (P_{(t-1)} + \Sigma_l)H^T(H(P_{(t-1)} + \Sigma_l)H^T + \Sigma_y)^{-1} \end{aligned} \quad (8)$$

where I_d is the identity matrix, P denotes the covariance matrix of the voltage state estimate \hat{V} , and K is the Kalman gain matrix minimizing the resulting covariance P : $K_{(t)} = \arg \min_K \text{trace}(P_{(t)})$.

Remark 2: Note that we are assuming that the noise $\omega_{l,(t)}$ in (7) has 0 mean. This is not necessary true since the loads could drift in expectation depending on the hour of the day. However, similarly as in Remark 1, on the considered fast time scales, this drift tends to 0 and can be neglected. We will observe this later in the test case in Section IV. Nevertheless, this work could be extended to a more general case with non-zero mean and also time dependent noise parameters: $\omega_{l,(t)} \sim \mathcal{N}(\mu_{l,(t)}, \Sigma_{l,(t)})$.

B. Convergence of the Projected Gradient Descent

Instead of using the state V as feedback as in (6), we use \hat{V} from (8) as input to the projected gradient descent:

$$S_{c,(t+1)} = \Pi_{\mathcal{F}}[S_{c,(t)} - \epsilon(\nabla_{S_c} f(S_{c,(t)}) + B_c^T \nabla_V g(\hat{V}_{(t)}))] \quad (9)$$

The interconnection of these subsystems (8) and (9) with the stochastic dynamic system of the grid (7) and the measurement equation (5), results in the closed-loop system represented in Fig. 1. However, even if the subsystems, SE (8) and the online feedback optimization (9), are both separately stable and converge to their optimal and true value, this does not

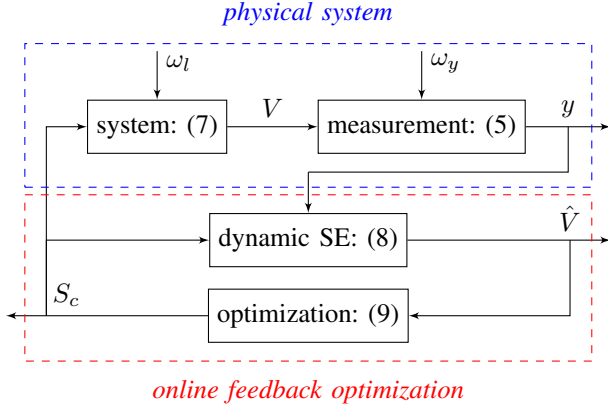


Fig. 1: Block diagram of interconnected systems stochastic dynamic system of distribution grid (7), measurements (5), SE (8) and online feedback optimization (9). Dashed square indicates the blocks of the online feedback optimization

guarantee that their interconnection will inherit these properties. Therefore, we need to verify the overall stability to ensure the desired behaviour of our approach.

Assumption 1: For proving this stability and convergence we need the following technical assumptions:

- 1) Both functions $f(\cdot), g(\cdot)$ have Lipschitz continuous gradients with parameters L_f, L_g respectively (i.e. $\|\nabla_{S_c} f(S_{c,1}) - \nabla_{S_c} f(S_{c,2})\|_2 \leq L_f \|S_{c,1} - S_{c,2}\|_2$, $\|\nabla_V g(V_1) - \nabla_V g(V_2)\|_2 \leq L_g \|V_1 - V_2\|_2$)
- 2) The function $g(\cdot)$ is convex
- 3) The function $f(\cdot)$ is η -strongly-convex (i.e. $(\nabla_{S_c} f(S_{c,1}) - \nabla_{S_c} f(S_{c,2}))^T (S_{c,1} - S_{c,2}) \geq \eta \|S_{c,1} - S_{c,2}\|_2^2$ or equivalently $f(S_c) - \frac{\eta}{2} \|S_c\|_2^2$ is convex).
- 4) The noise covariance matrices Σ_y, Σ_l have full rank.
- 5) The matrix $[B_c, B_l]$ has full-column rank.

The gradient Lipschitz continuity assumption is standard and typically true for most functions used for these kind of applications; convexity of $g(\cdot)$ will usually hold if using penalization functions like the one we described after (2); the strong convexity of $f(\cdot)$ could always be enforced by adding some quadratic regularization term to the objective function, see [2]. The full rank of the covariance matrices is to be expected, since although possibly correlated, each noise has a different source. Finally, the full-rank $[B_c, B_l]$ is generally true unless having zero-injection nodes. But in that case, a Kron reduction can be applied to the grid to eliminate those nodes.

Given the convexity of $f(\cdot), g(\cdot)$, we can then define the instantaneous global optimal value of (4) $S_{c,(t)}^*$ at time (t) , depending on the stochastic realization of $S_{l,(t)}$ at time (t) ; and $S_c^{\mathbb{E}*}$ the expected global optimal value using the expected loads $\mathbb{E}[S_{l,(t)}]$ in (4). Since $\mathbb{E}[\omega_{l,(t)}] = 0$, $\mathbb{E}[S_{l,(t)}]$ is independent of time (t) and so is $S_c^{\mathbb{E}*}$.

Theorem 1: Under Assumption 1 and choosing a step size $\epsilon < \frac{2\eta}{(L_f + \|B_c\|_2^2 L_g)^2 + \|B_c\|_2^2 L_g^2}$, the system in Fig. 1 has following stability and convergence results:

- Exponential convergence towards the unbiased and optimal solution: there exist constants $C_{V,1}, C_{V,2}, C_{S,1}, C_{V,2} > 0$ such that

$$\begin{aligned} & \|\hat{V}_{(t)} - \mathbb{E}[V_{(t)}]\|_2^2 \\ & \leq C_{V,1} e^{-C_{V,2}t} \|\hat{V}_{(0)} - \mathbb{E}[V_{(0)}]\|_2^2 \xrightarrow{t \rightarrow \infty} 0 \\ & \|S_{c,(t)} - S_c^{\mathbb{E}*}\|_2 \\ & \leq \sqrt{t} C_{S,1} e^{-C_{S,2}t} \|S_{c,(0)} - S_c^{\mathbb{E}*}\|_2 \xrightarrow{t \rightarrow \infty} 0 \end{aligned} \quad (10)$$

- Exponential bounded mean square (stochastic stability): there exist constants $C_V, C_{V,3}, C_{V,4}, C_S, C_{S,3}, C_{V,4} > 0$ such that

$$\begin{aligned} & \mathbb{E}[\|\hat{V}_{(t)} - V_{(t)}\|_2^2] \\ & \leq C_V + C_{V,3} e^{-C_{V,4}t} \mathbb{E}[\|\hat{V}_{(0)} - V_{(0)}\|_2^2] \xrightarrow{t \rightarrow \infty} C_V < \infty \\ & \mathbb{E}[\|S_{c,(t)} - S_c^{\mathbb{E}*}\|_2^2] \\ & \leq C_S + \sqrt{t} C_{S,3} e^{-C_{S,4}t} \mathbb{E}[\|S_{c,(0)} - S_c^{\mathbb{E}*}\|_2^2] \\ & \xrightarrow{t \rightarrow \infty} C_S < \infty, \end{aligned} \quad (11)$$

Both error terms $\hat{V}_{(t)} - V_{(t)}$ and $S_{c,(t)} - S_c^{\mathbb{E}*}$ are stochastic processes that quantify the estimation and the optimality deviation respectively. The first result (10) establishes that the expected values of these errors converge towards 0, while the second result (11) bounds the covariance of these errors. Both are required to conclude that the dynamic stochastic closed-loop process converges and is stable. Note that the convergence of $\hat{V}_{(t)} - V_{(t)}$ is faster than the one of $S_{c,(t)} - S_c^{\mathbb{E}*}$ due to the \sqrt{t} multiplying the exponential in the later case.

Given (3), $V_{(t)} - V_{(t)}^* = B_c(S_{c,(t)} - S_{c,(t)}^*)$ and $\mathbb{E}[V_{(t)}] - V_{(t)}^{\mathbb{E}*} = B_c(S_{c,(t)} - S_{c,(t)}^{\mathbb{E}*})$, so the convergence of $V_{(t)}$ is a result of the convergence of $S_{c,(t)}$.

These constants $C_V, C_S, C_{V,(\cdot)}, C_{S,(\cdot)}$ depend on the parameters $\eta, L_f, L_g, B_c, B_l, H$, and the noise covariances Σ_l, Σ_y . Their expressions can be found in the proof in Appendix A. Moreover, C_V, C_S are linear combinations of functions of $\text{trace}(\Sigma_l), \text{trace}(\Sigma_y)$ for the estimation error or $\sqrt{\text{trace}(\Sigma_l)}, \sqrt{\text{trace}(\Sigma_y)}$ for the optimization error. This means that if these terms can be lowered, so will the error bound. Intuitively, this could be expected to happen if using faster time scales.

IV. TEST CASE

We validate our proposed method by simulating the behaviour of a test distribution grid during 30 minutes with 1-second time intervals (1800 iterations). Here we describe the settings of the test case and analyse the results. The algorithms are coded in Python and run on an Intel Core i7-8750H CPU at 2.20GHz with 16GB of RAM.

A. Settings

Simulation data settings:

- System: We use the IEEE 123-bus test feeder available online [10], see Fig. 2.
- Load Profiles: We use the 1-second resolution data of the ECO data set [15]. To adapt it to this grid, we first

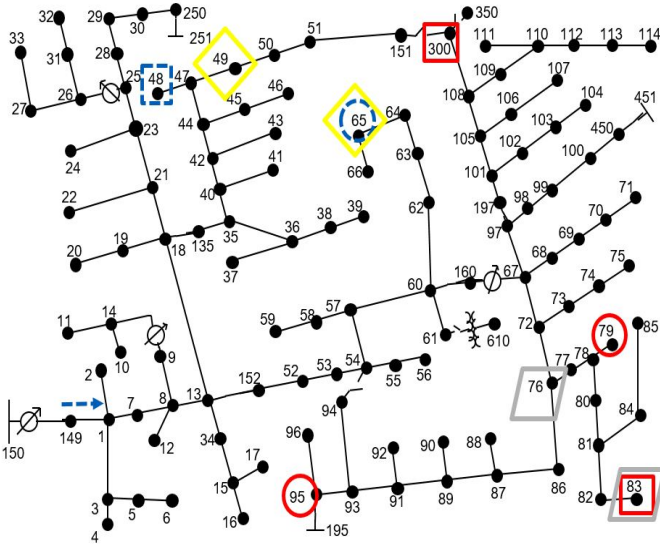


Fig. 2: 123-bus test feeder [10] with location of measurements and distributed generation marked.

aggregate over some households and rescale it to have similar values as the base loads of the 123-bus feeder.

- Measurements for the SE (see Fig. 2): Similar to [8], voltage measurements (red circle for phasor, red square for magnitude only) are placed at buses 95, 79, 300 and 83, current measurements (blue dashed circle for phasor, blue dashed square for magnitude only) at buses 65 and 48, and branch current phasor measurements (blue dashed arrow) at branch 149-1 after the regulator. As in [8], we assign a relatively low value (1%) to the covariance terms in Σ_y corresponding to these measurements.
- Pseudo-measurements: We build these profiles by simply averaging the load profiles in the ECO data set [15]. As in [8], we assign a relatively high value (50%) to the covariance terms in Σ_y corresponding to these measurements.
- Distributed Generation: Similar to [9], solar energy is introduced in the three phases of nodes 49 and 65, and wind energy in nodes 76 and 83, see Fig 2 (a yellow rhombus for solar, a grey parallelogram for wind). Their profiles are simulated using a 1-minute solar irradiation profile and a 2-minute wind speed profiles from [16], [17]. To adapt this 1,2-minute resolution data to the 1-second consumption data, we hold the values constant during all seconds within every single minute interval.

Optimization settings:

- Objective function $f(S_c)$: We consider a quadratic cost on the controllable resources that penalises not using all the available active power in the renewable resources, and also using any reactive power: $f_i((P, Q)_{c,i}) = (P_{c,i} - P_{i,\max})^T (P_{c,i} - P_{i,\max}) + Q_{c,i}^T Q_{c,i}$. This function is strongly convex and has a Lipschitz continuous gradient with parameters $\eta = L_f = 1$.
- Objective function $g(V)$: As mentioned after (2), we use

a $g(V)$ penalizing voltage violations, with parameter $\rho = 100$. This function is convex and its gradient is Lipschitz continuous with parameter $L_g = 100$. We use the voltage limits $V_{\max} = 1.06$ p.u. and $V_{\min} = 0.94$ p.u. as in [4].

- Feasible space \mathcal{F} : We consider a feasible space limiting both the active and reactive power: $\mathcal{F} = \{S_c | 0 \leq P_{c,i} \leq P_{i,\max}, Q_{i,\min} \leq Q_{c,i} \leq Q_{i,\max}\}$. This could easily be extended to more complex feasible space using the projection proposed in [2].
- Descent rate: Experimentally, we have found that with a descent rate $\epsilon = 0.001$ the proposed method converges and remains stable.

B. Results

Given the theoretical result presented in Theorem 1, we monitor the optimization error norm $\|S_{c,(t)} - S_{c,(t)}^*\|_2$, and the estimation error norm $\|\hat{V}_{(t)} - V_{(t)}^*\|_2$. The first to observe in Fig. 3 is that, with the settings described, the optimization error converges in approximately 20 min (1200 iterations) and remains stable. In the estimation, Fig. 4 shows how the error reduces very quickly in a few seconds (few iterations) and then remains stable at less than 1%. These observations coincide with the results (11) in Theorem 1, since the expected value of the norm is bounded, but not necessarily converges to 0. Despite that, it converges to close to 0. This is a consequence of using fast time scales and thus low covariances Σ_l, Σ_y , which in turn produce low constant bounds C_V, C_S . Moreover, as mentioned in the Theorem 1, the difference in the number of iterations required to converge, is a result of the term \sqrt{t} multiply the exponential part of the bound for the set-points case in (10) and (11).

Nonetheless, it is remarkable that we observe an accurate convergence as predicted by Theorem 1, despite the fact that our theoretical assumption of zero mean process noise $\omega_{l,(t)}$ in (7) is not necessarily met for the true consumption data [15] used in this simulation. This supports the statement in Remark 2 that for fast time-scales this drift can be neglected. Similarly for Remark 1, the feasible set \mathcal{F} that we have used is not constant due to the time-varying profiles in solar radiation and wind speed [16], [17]. However, this has not affected the convergence of our method, because the changes in \mathcal{F} are also negligible at these fast time-scales. Additionally, thanks to using a large standard deviation for the pseudo-measurements, the effect of a potential bias in their error is diminished and the convergence is not affected.

Moreover, we obtain this accurate convergence despite the potential error due to the linear approximation done in (3) and (5). This is a consequence of using the real-time feedback optimization, since its robustness helps to correct potential model mismatches.

Finally, it can be observed in Fig. 5 that the voltage magnitude values remain within limits almost all the time for every node. There are small violations, which may be due to the estimation uncertainty represented in the covariance matrix $P_{(t)}$ in (8), and the fact that we are not enforcing hard state constraints in (4), but only penalising their violations.

V. CONCLUSIONS

In this paper we have proposed how to add a dynamic State Estimation (SE) to the online feedback optimization of the Optimal Power Flow (OPF). We have formally proven that the interconnected system of SE and feedback optimization is stochastically stable and converges to the true state and optimal solution, respectively. Moreover, we have observed in a simulated test case how our method succeeds in driving the controllable elements towards near-optimal set-points while keeping an accurate state estimate.

Future work could include taking into account the uncertainty represented in the estimation error covariance matrix for a better control of the voltage states, considering a nonlinear power flow and measurements equation, or considering a time-varying case and biased pseudo-measurements.

REFERENCES

- [1] S. Bolognani, R. Carli, G. Cavraro, and S. Zampieri, "Distributed reactive power feedback control for voltage regulation and loss minimization," *IEEE Transactions on Automatic Control*, vol. 60, no. 4, pp. 966–981, April 2015.
- [2] E. Dall'Anese and A. Simonetto, "Optimal power flow pursuit," *IEEE Transactions on Smart Grid*, vol. 9, no. 2, pp. 942–952, March 2018.
- [3] D. K. Molzahn, F. Drfler, H. Sandberg, S. H. Low, S. Chakrabarti, R. Baldick, and J. Lavaei, "A survey of distributed optimization and control algorithms for electric power systems," *IEEE Transactions on Smart Grid*, vol. 8, no. 6, pp. 2941–2962, Nov 2017.
- [4] A. Hauswirth, A. Zanardi, S. Bolognani, F. Dörfler, and G. Hug, "Online optimization in closed loop on the power flow manifold," in *2017 IEEE Manchester PowerTech*, June 2017, pp. 1–6.
- [5] M. Colombino, E. Dall'Anese, and A. Bernstein, "Online optimization as a feedback controller: Stability and tracking," *IEEE Transactions on Control of Network Systems*, pp. 1–1, 2019, in press.
- [6] A. Abur and A. G. Exposito, *Power System State Estimation: Theory and Implementation*. CRC Press, 2004.
- [7] L. Schenato, G. Barchi, D. Macii, R. Arghandeh, K. Poolla, and A. V. Meier, "Bayesian linear state estimation using smart meters and pmus measurements in distribution grids," in *IEEE International Conference on Smart Grid Communications*, Nov 2014, pp. 572–577.
- [8] M. Picallo, A. Anta, A. Panosyan, and B. De Schutter, "A two-step distribution system state estimator with grid constraints and mixed measurements," in *IEEE Power Systems Computation Conference*, June 2018.
- [9] M. Picallo, A. Anta, and B. De Schutter, "Stochastic optimal power flow in distribution grids under uncertainty from state estimation," in *IEEE Conference on Decision and Control*, Dec 2018.
- [10] W. Kersting, "Radial distribution test feeders," *IEEE Transactions on Power Systems*, vol. 6, no. 3, pp. 975–985, 1991.
- [11] S. H. Low, "Convex relaxation of optimal power flowpart ii: Exactness," *IEEE Transactions on Control of Network Systems*, vol. 1, no. 2, pp. 177–189, June 2014.
- [12] S. Bolognani and S. Zampieri, "On the existence and linear approximation of the power flow solution in power distribution networks," *IEEE Transactions on Power Systems*, vol. 31, no. 1, pp. 163–172, 2016.
- [13] T. Baldwin, L. Mili, M. Boisen, and R. Adapa, "Power system observability with minimal phasor measurement placement," *IEEE Transactions on Power Systems*, vol. 8, no. 2, pp. 707–715, 1993.
- [14] A. Monticelli, "Electric power system state estimation," *Proceedings of the IEEE*, vol. 88, no. 2, pp. 262–282, 2000.
- [15] C. Beckel, W. Kleiminger, R. Cicchetti, T. Staake, and S. Santini, "The ECO data set and the performance of non-intrusive load monitoring algorithms," in *Proceedings of the 1st ACM Conference on Embedded Systems for Energy-Efficient Buildings*, 11 2014.
- [16] HelioClim-3, "HelioClim-3 Database of Solar Irradiance," <http://www.soda-pro.com/web-services/radiation/helioclim-3-archives-for-free>, [Online]. Accessed: 2017-12-01.
- [17] MERRA-2, "The Modern-Era Retrospective analysis for Research and Applications, Version 2 (MERRA-2) Web service," <http://www.soda-pro.com/web-services/meteo-data/merra>, [Online]. Accessed: 2017-12-01.

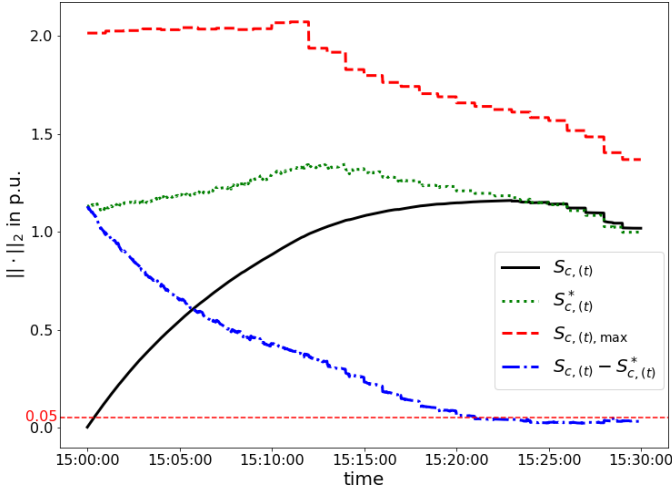


Fig. 3: Norm at each time instant (t) of the proposed set-points $S_{c,t}(t)$, the optimum $S_{c,t}^*(t)$, the maximum power available $S_{c,t}(t),max$ according to the feasible set \mathcal{F} , and the optimality error $S_{c,t}(t) - S_{c,t}^*(t)$. A line marks how the error stabilizes around 0.05p.u.

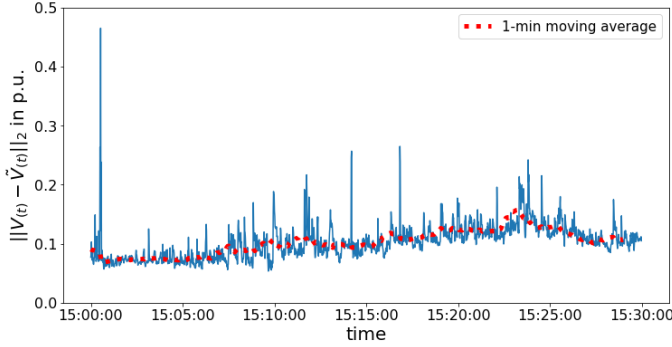


Fig. 4: Norm at each time instant (t) of the error between the estimated state $\hat{V}(t)$ and the true state $V(t)$.

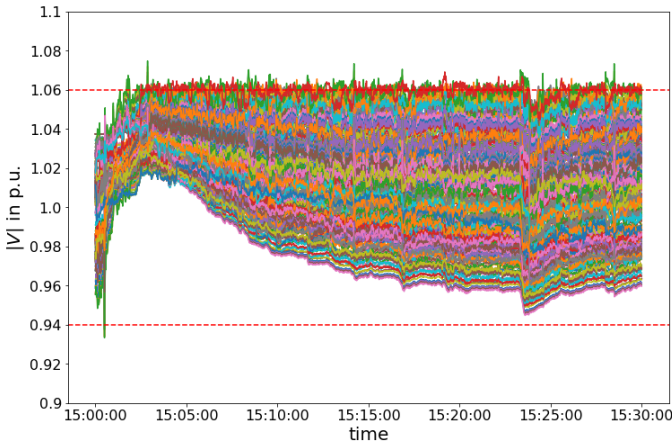


Fig. 5: Magnitude at each time instant (t) of the true voltage value $V(t)$ for every node during the simulation time.

- [18] M. Fazlyab, A. Ribeiro, M. Morari, and V. Preciado, "Analysis of optimization algorithms via integral quadratic constraints: Nonstrongly convex problems," *SIAM Journal on Optimization*, vol. 28, no. 3, pp. 2654–2689, 2018.
- [19] Tzyh-Jong Tarn and Y. Rasis, "Observers for nonlinear stochastic systems," *IEEE Transactions on Automatic Control*, vol. 21, no. 4, pp. 441–448, August 1976.
- [20] A. H. Jazwinski, "Mathematics in science and engineering," *Stochastic processes and filtering theory*, vol. 64, 1970.
- [21] K. J. Åström, *Introduction to stochastic control theory*. Courier Corporation, 2012.
- [22] K. Reif, S. Gunther, E. Yaz, and R. Unbehauen, "Stochastic stability of the discrete-time extended kalman filter," *IEEE Transactions on Automatic Control*, vol. 44, no. 4, pp. 714–728, April 1999.
- [23] M. A. Woodbury, "Inverting modified matrices," *Statistical Research Group Memorandum Reports*. Princeton, NJ: Princeton University, no. 42, 1950.

APPENDIX A PROOF OF THEOREM 1

For the proof, we first write the whole closed-loop system in Fig. 1 connecting together all the parts in (5), (7), (8), (9). Denoting the estimation error as $e(t) = \hat{V}(t) - V(t)$, we define the state $x(t)$, output $z(t)$, and disturbance $\omega(t)$ as

$$x(t) = \begin{bmatrix} V(t) \\ e(t) \\ S_{c,(t)} \end{bmatrix}, z(t) = \begin{bmatrix} \hat{V}(t) \\ S_{c,(t)} \end{bmatrix}, \omega(t) = \begin{bmatrix} \omega_{l,(t)} \\ \omega_{y,(t)} \end{bmatrix} \quad (12)$$

Next we define the control input $u_{(t+1)} = \phi_\epsilon(z(t))$, depending on the output $z(t)$ through the nonlinear feedback $\phi_\epsilon(\cdot)$. This operator $\phi_\epsilon(\cdot)$ is the generalized gradient mapping [18] adapted to the projected gradient descent in (9), and it is a mere reformulation of (9):

$$\phi_\epsilon(z) = \frac{1}{\epsilon} (S_c - \Pi_{\mathcal{F}} [S_c - \epsilon (\nabla_{S_c} f(S_c) + B_c^T \nabla_V g(\hat{V}))]) \quad (13)$$

As a result, we get the nonlinear stochastic closed-loop interconnected system represented in Fig. 1 and expressed as

$$\begin{aligned} x_{(t+1)} &= \begin{bmatrix} I_d & 0 & 0 \\ 0 & I_d - K_{(t+1)}H & 0 \\ 0 & 0 & I_d \end{bmatrix} x_{(t)} + \begin{bmatrix} -\epsilon B_l \\ 0 \\ -\epsilon I_d \end{bmatrix} u_{(t+1)} \\ &\quad + \begin{bmatrix} B_l & 0 \\ -(I_d - K_{(t+1)}H)B_l & K_{(t+1)} \\ 0 & 0 \end{bmatrix} \omega_{(t+1)} \\ z_{(t)} &= \begin{bmatrix} I_d & I_d & 0 \\ 0 & 0 & I_d \end{bmatrix} x_{(t)} \\ u_{(t+1)} &= \phi_\epsilon(z_{(t)}). \end{aligned} \quad (14)$$

Considering a perfect estimation $e_{(t)}^* = 0$, and using the instantaneous and expected global optimal values defined before Theorem 1, $S_{c,(t)}^*$ and $S_{c,(t)}^{\mathbb{E}*}$ respectively, we can define the desired points $x_{(t)}^* = [(V_{(t)}^*)^T, 0, (S_{c,(t)}^*)^T]^T$ and $x_{(t)}^{\mathbb{E}*} = [(V_{(t)}^{\mathbb{E}*})^T, 0, (S_{c,(t)}^{\mathbb{E}*})^T]^T$. Due to optimality, these points are instantaneous fixed points of the projected gradient descent. Then, at these points $\phi_\epsilon(z_{(t)}^*) = 0$, $\phi_\epsilon(z_{(t)}^{\mathbb{E}*}) = 0$, and thus $x_{(t)}^{\mathbb{E}*}$ is an equilibrium point, and $x_{(t)}^*$ are instantaneous equilibrium

points at each time (t) . Next, we analyse the stability of these points to prove the convergence of (8) and (9).

A. Proof of (11)

We start formulating some results:

Lemma 1: The objective as a function of S_c : $\tilde{f}(S_c) = f(S_c) + g(V(S_c)) = f(S_c) + g(V_0 + B_c S_c + B_l S_l)$ is η -strongly convex and has a Lipschitz continuous gradient with parameter $L = L_f + \|B_c\|_2^2 L_g$.

Proof:

- 1) Strongly convex: Since $g(V)$ is convex on V , $g(V_0 + B_c S_c + B_l S_l)$ is convex on S_c . Then, since $f(S_c)$ is η -strongly convex, so is $\tilde{f}(S_c)$.
- 2) Lipschitz: We have $\nabla_{S_c} \tilde{f}(S_c) = \nabla_{S_c} f(S_c) + B_c^T \nabla_V g(V_0 + B_c S_c + B_l S_l)$, then

$$\begin{aligned} &\|\nabla_{S_c} \tilde{f}(S_{c,1}) - \nabla_{S_c} \tilde{f}(S_{c,2})\|_2 \\ &\leq L_f \|S_{c,1} - S_{c,2}\|_2 + \|B_c\|_2 L_g \|B_c(S_{c,1} - S_{c,2})\|_2 \\ &\leq (L_f + \|B_c\|_2^2 L_g) \|S_{c,1} - S_{c,2}\|_2 \end{aligned} \quad (15)$$

Lemma 2: There exists a Lipschitz constant $L_{S,\text{opt}}$, such that the operators mapping the subsequent values $S_{l,(t)}, S_{l,(t+1)}$, to the respective optimal solutions $S_{c,(t)}^*, S_{c,(t+1)}^*$ of (4) satisfy:

$$\|S_{c,(t+1)}^* - S_{c,(t)}^*\|_2 \leq L_{S,\text{opt}} \|B_l(S_{l,(t+1)} - S_{l,(t)})\|_2 \quad (16)$$

Proof: The proof is in Appendix B. ■

Theorem 2: [19, Theorem 2] If there is a stochastic process $z_{(t)}$, a function $\mathcal{V}_{(t)}(\cdot)$ and real numbers $\tilde{\nu}, \hat{\nu}, \zeta > 0$ and $0 < \delta \leq 1$ such that

$$\tilde{\nu} \|z_{(t)}\|_2^2 \leq \mathcal{V}_{(t)}(z_{(t)}) \leq \hat{\nu} \|z_{(t)}\|_2^2 \quad (17a)$$

$$\mathbb{E}[\mathcal{V}_{(t+1)}(z_{(t+1)}) | \mathcal{V}_{(t)}(z_{(t)})] \leq \zeta + (1 - \delta) \mathcal{V}_{(t)}(z_{(t)}) \quad (17b)$$

then

$$\begin{aligned} \mathbb{E}[\|z_{(t)}\|_2^2] &\leq \frac{\hat{\nu}}{\tilde{\nu}} \mathbb{E}[\|z_{(0)}\|_2^2] (1 - \delta)^t + \frac{\zeta}{\tilde{\nu}} \sum_{i=1}^{t-1} (1 - \delta)^i \\ &\leq \frac{\hat{\nu}}{\tilde{\nu}} \mathbb{E}[\|z_{(0)}\|_2^2] (1 - \delta)^t + \frac{\zeta}{\tilde{\nu} \delta}, \end{aligned}$$

According to Assumption 1, H and $[B_c, B_l]$ have full-column rank, and Σ_y, Σ_l full rank. Given also that the measurement matrix H in (5) has full-column rank with the pseudo-measurements, the system is uniformly completely observable and controllable [20, Chapter 7]. Thus, the covariance matrix $P_{(t)}$ is upper and lower bounded for all (t) [20, Lemma 7.1 and 7.2], i.e., there exist parameters $\check{\sigma}, \hat{\sigma} > 0$, depending on $\Sigma_l, \Sigma_y, H, B_c, B_l$, that bound $P_{(t)}$, so that: $\check{\sigma} I_d \preceq P_{(t)} \preceq \hat{\sigma} I_d \forall t$. As a result, $K_{(t)}$ is also bounded.

Since we have a linear open-loop system (7) and estimator (8), the separation principle [21] holds and we can analyse the stability and convergence of the estimator and controller separately, despite the non-linear feedback. Then, using the *Lyapunov* function $\mathcal{V}_{(t)}(e_{(t)}) = e_{(t)}^T P_{(t)}^{-1} e_{(t)}$, we can prove the results of Theorem 1 for the estimation error $e(t)$: The first

condition (17a) is satisfied using the bounds of $P_{(t)}$, and (17b) can be proven using a similar reasoning as in [22]:

$$\begin{aligned}
& e_{(t+1)}^T P_{(t+1)}^{-1} e_{(t+1)} \\
\stackrel{a)}{=} & e_{(t)}^T (I_d - K_{(t+1)} H)^T P_{(t+1)}^{-1} (I_d - K_{(t+1)} H) e_{(t)} \\
& + \omega_{y,(t+1)}^T K_{(t+1)}^T P_{(t+1)}^{-1} K_{(t+1)} \omega_{y,(t+1)} \\
& + \omega_{l,(t+1)}^T (I_d - K_{(t+1)} H)^T P_{(t+1)}^{-1} (I_d - K_{(t+1)} H) \omega_{l,(t+1)} \\
& + (\text{crossed terms on } e_{(t)}, \omega_{y,(t)}, \omega_{l,(t)}) \\
\stackrel{b)}{=} & e_{(t)}^T (P_{(t)} + \Sigma_l)^{-1} (I_d - K_{(t+1)} H) e_{(t)} \\
& + \omega_{y,(t+1)}^T K_{(t+1)}^T P_{(t+1)}^{-1} K_{(t+1)} \omega_{y,(t+1)} \\
& + \omega_{l,(t+1)}^T (I_d - K_{(t+1)} H)^T P_{(t+1)}^{-1} (I_d - K_{(t+1)} H) \omega_{l,(t+1)} \\
& + (\text{crossed terms on } e_{(t)}, \omega_{y,(t)}, \omega_{l,(t)}) \\
\stackrel{c)}{=} & e_{(t)}^T P_{(t)}^{-1} e_{(t)} \\
& - e_{(t)}^T P_{(t)}^{-1} (P_{(t)}^{-1} + \Sigma_l^{-1})^{-1} P_{(t)}^{-1} e_{(t)} \\
& - e_{(t)}^T H^T (H(P_{(t)} + \Sigma_l) H^T + \Sigma_y)^{-1} H e_{(t)} \\
& + \omega_{y,(t+1)}^T K_{(t+1)}^T P_{(t+1)}^{-1} K_{(t+1)} \omega_{y,(t+1)} \\
& + \omega_{l,(t+1)}^T (I_d - K_{(t+1)} H)^T P_{(t+1)}^{-1} (I_d - K_{(t+1)} H) \omega_{l,(t+1)} \\
& + (\text{crossed terms on } e_{(t)}, \omega_{y,(t)}, \omega_{l,(t)}) \\
\stackrel{d)}{\leq} & e_{(t)}^T P_{(t)}^{-1} e_{(t)} - \psi \|e_{(t)}\|_2^2 \\
& + \frac{1}{\hat{\sigma}} (\|K_{(t+1)} \omega_{y,(t)}\|_2^2 + \|(I_d - K_{(t+1)} H) \omega_{l,(t)}\|_2^2) \\
& + (\text{crossed terms on } e_{(t)}, \omega_{y,(t)}, \omega_{l,(t)}) \\
\stackrel{e)}{=} & (1 - \psi \hat{\sigma}) e_{(t)}^T P_{(t)}^{-1} e_{(t)} \\
& + \frac{1}{\hat{\sigma}} (\|K_{(t+1)} \omega_{y,(t)}\|_2^2 + \|(I_d - K_{(t+1)} H) \omega_{l,(t)}\|_2^2) \\
& + (\text{crossed terms on } e_{(t)}, \omega_{y,(t)}, \omega_{l,(t)})
\end{aligned} \tag{18}$$

where in *a*) we have expanded $e_{(t+1)}$ using (14); in *b*) we have used the expression of $P_{(t+1)}$ in (8); in *c*) we use Woodbury matrix identity [23] on $(P_{(t)} + \Sigma_l)^{-1}$, and the expression of $K_{(t+1)}$ in (8); in *d*) we use the upper bound of $P_{(t+1)}^{-1}$, and that since $P_{(t)}^{-1} (P_{(t)}^{-1} + \Sigma_l^{-1})^{-1} P_{(t)}^{-1} \succ 0$, $H^T (H(P_{(t)} + \Sigma_l) H^T + \Sigma_y)^{-1} H \succ 0$, there exists $\psi > 0$ such that *d*) is true, with:

$$\begin{aligned}
\psi \leq & \lambda_{\min} \left(P_{(t)}^{-1} (P_{(t)}^{-1} + \Sigma_l^{-1})^{-1} P_{(t)}^{-1} \right. \\
& \left. + H^T (H(P_{(t)} + \Sigma_l) H^T + \Sigma_y)^{-1} H \right)
\end{aligned} \tag{19}$$

where $\lambda_{\min}(\cdot)$ denote the minimum eigenvalue; and in *e*) we use the upper bound of $P_{(t)}$. Note that (19) provides an upper bound on ψ , so we can choose ψ such that $\psi \hat{\sigma} < 1$. Taking the expectation $\mathbb{E}[\cdot]$, since $\mathbb{E}[\omega_{y,(t)}] = \mathbb{E}[\omega_{l,(t)}] = 0$, the crossed terms vanish and we get:

$$\begin{aligned}
& \mathbb{E}[e_{(t+1)}^T P_{(t+1)}^{-1} e_{(t+1)} \mid e_{(t)}^T P_{(t)}^{-1} e_{(t)}] \\
& \leq (1 - \psi \hat{\sigma}) e_{(t)}^T P_{(t)}^{-1} e_{(t)} + \tau (\text{trace}(\Sigma_y) + \text{trace}(\Sigma_l))
\end{aligned} \tag{20}$$

where we have used $\mathbb{E}[\|\omega_{(\cdot),(t)}\|_2^2] = \text{trace}(\Sigma_{(\cdot)})$, and $\tau = \frac{1}{\hat{\sigma}} \max(\|K_{(t+1)}\|_2^2, \|I_d - K_{(t+1)} H\|_2^2) < \infty$. Then, we can conclude that $e_{(t)}$ is exponentially bounded in mean square

and provide the corresponding bound (11) using Theorem 2:

$$\begin{aligned}
& \mathbb{E}[\|e_{(t)}\|_2^2] \\
& \leq \frac{\hat{\sigma}}{\psi} (1 - \psi \hat{\sigma})^t \mathbb{E}[\|e_{(0)}\|_2^2] + \frac{\tau}{\psi} (\text{trace}(\Sigma_y) + \text{trace}(\Sigma_l)) \\
& \xrightarrow{t \rightarrow \infty} \frac{\tau}{\psi} (\text{trace}(\Sigma_y) + \text{trace}(\Sigma_l))
\end{aligned} \tag{21}$$

Next we study at the convergence and stability of $S_{c,(t)}$. Due to Lemma 2, we have

$$\begin{aligned}
& \|S_{c,(t+1)} - S_{c,(t+1)}^*\|_2 \\
& \leq \|S_{c,(t+1)} - S_{c,(t)}^*\|_2 + \|S_{c,(t)}^* - S_{c,(t)}^*\|_2 \\
& \leq \|S_{c,(t+1)} - S_{c,(t)}^*\|_2 + L_{S,\text{opt}} \|B_l(S_{l,(t+1)} - S_{l,(t)})\|_2 \\
& \leq \|S_{c,(t+1)} - S_{c,(t)}^*\|_2 + L_{S,\text{opt}} \|\omega_{l,(t+1)}\|_2
\end{aligned} \tag{22}$$

Then we have

$$\begin{aligned}
& \|S_{c,(t+1)} - S_{c,(t)}^*\|_2 \\
\stackrel{a)}{=} & \|\Pi_{\mathcal{F}}[S_{c,(t)} - \epsilon(\nabla_{S_c} f(S_{c,(t)}) + B_c^T \nabla_V g(\hat{V}_{(t)}))] \\
& - \Pi_{\mathcal{F}}[S_{c,(t)}^* - \epsilon(\nabla_{S_c} f(S_{c,(t)}^*) + B_c^T \nabla_V g(V_{(t)}^*))]\|_2 \\
\stackrel{b)}{\leq} & \|S_{c,(t)} - \epsilon(\nabla_{S_c} f(S_{c,(t)}) + B_c^T \nabla_V g(\hat{V}_{(t)})) \\
& - S_{c,(t)}^* + \epsilon(\nabla_{S_c} f(S_{c,(t)}^*) + B_c^T \nabla_V g(V_{(t)}^*))\|_2 \\
\stackrel{c)}{\leq} & \|S_{c,(t)} - S_{c,(t)}^* - \epsilon(\nabla_{S_c} f(S_{c,(t)}) - \nabla_{S_c} f(S_{c,(t)}^*)) \\
& + B_c^T \nabla_V g(V_{(t)}) - B_c^T \nabla_V g(V_{(t)}^*)\|_2 \\
& + \|\epsilon B_c^T (\nabla_V g(\hat{V}_{(t)}) - \nabla_V g(V_{(t)}))\|_2 \\
\stackrel{d)}{\leq} & \sqrt{1 - 2\eta\epsilon + \epsilon^2 L^2} \|S_{c,(t)} - S_{c,(t)}^*\|_2 + \epsilon \|B_c\|_2 L_g \|e_{(t)}\|_2
\end{aligned} \tag{23}$$

where in *a*) we use that $S_{c,(t)}^*$ is a fixed point of the projected gradient descent (9) due to its optimality; in *b*) we remove the projection; in *c*) we add and subtract $\epsilon B_c^T \nabla_V g(V_{(t)})$, and then use the triangle inequality; in *d*), for the first norm we use the strong convexity and the Lipschitz continuity given by Lemma 1; and for the second norm the Lipschitz continuity of $\nabla_V g(V)$. Defining $r(\epsilon) = \sqrt{1 - 2\eta\epsilon + \epsilon^2 L^2}$, we combine (22) and (23), and take expectations to get:

$$\begin{aligned}
& \mathbb{E}[\|S_{c,(t+1)} - S_{c,(t+1)}^*\|_2] \\
& \leq r(\epsilon)\mathbb{E}[\|S_{c,(t)} - S_{c,(t)}^*\|_2] \\
& \quad + \epsilon\|B_c\|_2 L_g \mathbb{E}[\|e_{(t)}\|_2] + L_{S,\text{opt}} \mathbb{E}[\|\omega_{l,(t)}\|_2] \\
& \stackrel{a)}{\leq} r(\epsilon)^t \mathbb{E}[\|S_{c,(0)} - S_{c,(0)}^*\|_2] \\
& \quad + \sum_{k=0}^t r(\epsilon)^{(t-k)} (L_{S,\text{opt}} \sqrt{\text{trace}(\Sigma_l)} \\
& \quad + \epsilon\|B_c\|_2 L_g \sqrt{\mathbb{E}[\|e_{(k)}\|_2^2]}) \\
& \stackrel{b)}{\leq} r(\epsilon)^t \mathbb{E}[\|S_{c,(0)} - S_{c,(0)}^*\|_2] \\
& \quad + \sum_{k=0}^t r(\epsilon)^{(t-k)} \left(L_{S,\text{opt}} \sqrt{\text{trace}(\Sigma_l)} \right. \\
& \quad + \epsilon\|B_c\|_2 L_g \sqrt{\frac{\hat{\sigma}}{\sigma} (1 - \psi\hat{\sigma})^k \mathbb{E}[\|e_{(0)}\|_2^2]} \\
& \quad \left. + \epsilon\|B_c\|_2 L_g \sqrt{\frac{\tau}{\psi} (\text{trace}(\Sigma_y) + \text{trace}(\Sigma_l))} \right) \\
& \stackrel{c)}{\leq} r(\epsilon)^t \mathbb{E}[\|S_{c,(0)} - S_{c,(0)}^*\|_2] \\
& \quad + \frac{1}{1-r(\epsilon)} \left(L_{S,\text{opt}} \sqrt{\text{trace}(\Sigma_l)} \right. \\
& \quad + \epsilon\|B_c\|_2 L_g \sqrt{\frac{\tau}{\psi} (\text{trace}(\Sigma_y) + \text{trace}(\Sigma_l))} \\
& \quad + \epsilon\|B_c\|_2 L_g \sqrt{\frac{\hat{\sigma}}{\sigma} \mathbb{E}[\|e_{(0)}\|_2^2]} t \max(r(\epsilon), \sqrt{1 - \psi\hat{\sigma}})^t \Big) \\
& \stackrel{t \rightarrow \infty}{\rightarrow} \frac{1}{1-r(\epsilon)} \left(L_{S,\text{opt}} \sqrt{\text{trace}(\Sigma_l)} \right. \\
& \quad \left. + \epsilon\|B_c\|_2 L_g \sqrt{\frac{\tau}{\psi} (\text{trace}(\Sigma_y) + \text{trace}(\Sigma_l))} \right) \tag{24}
\end{aligned}$$

where in *a*) we apply the inequality in (23) (*t*)-times, and use the Jensen inequality for the concave function $\sqrt{(\cdot)}$ on $\mathbb{E}[\|\omega_{l,(t)}\|_2]$ and $\mathbb{E}[\|e_{(k)}\|_2]$: $\mathbb{E}[\|(\cdot)\|_2] \leq \sqrt{\mathbb{E}[\|(\cdot)\|_2^2]}$; in *b*) we substitute $\mathbb{E}[\|e_{(k)}\|_2^2]$ using (21) and use that $\sqrt{(\cdot)}$ is subadditive: $\sqrt{x+y} \leq \sqrt{x} + \sqrt{y}$, $\forall x, y > 0$; and in *c*) and the limit, we sum over *k* and use the following: $r(\epsilon) < 1$ if choosing a step size $\epsilon < \frac{2\eta}{(L_f + \|B_c\|_2^2 L_g)^2 + \|B_c\|_2^2 L_g^2}$ according to Theorem 1, given also that $1 - \psi\hat{\sigma} < 1$ as explained after (19), $r(\epsilon) > 1 - \frac{\eta^2}{L^2} > 0$, and $1 - \psi\hat{\sigma} > 0$, then $0 < r(\epsilon)^{t-k} \sqrt{1 - \psi\hat{\sigma}}^k \leq \max(r(\epsilon), \sqrt{1 - \psi\hat{\sigma}})^t$, with $\max(r(\epsilon), \sqrt{1 - \psi\hat{\sigma}}) < 1$.

B. Proof of (10)

Taking expectations on the interconnected system (14), we can eliminate the disturbance noise $\omega_{(t)}$. Without it and using the same procedure as before for the estimation part, we get a version of (20) without the constant term

$$\|\mathbb{E}[e_{(t)}]\|_2^2 \leq \frac{\hat{\sigma}}{\sigma} (1 - \psi\hat{\sigma})^t \|\mathbb{E}[e_{(0)}]\|_2^2 \xrightarrow{t \rightarrow \infty} 0, \tag{25}$$

and for the optimality part we have

$$\begin{aligned}
& \|S_{c,(t+1)} - S_{c,(t+1)}^{\mathbb{E}*}\|_2 \\
& \stackrel{a)}{\leq} r(\epsilon)\|S_{c,(t)} - S_{c,(t)}^{\mathbb{E}*}\|_2 + \epsilon\|B_c\|_2 L_g \|\mathbb{E}[e_{(t)}]\|_2 \\
& \stackrel{b)}{\leq} r(\epsilon)\|S_{c,(t)} - S_{c,(t)}^{\mathbb{E}*}\|_2 + \epsilon\|B_c\|_2 L_g \sqrt{\frac{\hat{\sigma}}{\sigma} \|\mathbb{E}[e_{(0)}]\|_2^2} \sqrt{1 - \psi\hat{\sigma}}^t \\
& \stackrel{c)}{\leq} r(\epsilon)^t \|S_{c,(0)} - S_{c,(0)}^{\mathbb{E}*}\|_2 \\
& \quad + \epsilon\|B_c\|_2 L_g \sqrt{\frac{\hat{\sigma}}{\sigma} \|\mathbb{E}[e_{(0)}]\|_2^2} t \max(r(\epsilon), \sqrt{1 - \psi\hat{\sigma}})^t \\
& \stackrel{t \rightarrow \infty}{\rightarrow} 0 \tag{26}
\end{aligned}$$

where in *a*) we use same arguments as in (23), but adding and subtracting $\epsilon B_c^T \nabla_V g(\mathbb{E}[V_{(t)}])$; in *b*) we substitute $\|\mathbb{E}[e_{(t)}]\|_2^2$ using (25); in *c*) we apply the previous inequality (*t*)-times and sum the terms as in (24)

APPENDIX B PROOF OF LEMMA 2

$$\begin{aligned}
& \|S_{c,(t+1)}^* - S_{c,(t)}^*\|_2 \\
& \stackrel{a)}{=} \|\Pi_{\mathcal{F}}[S_{c,(t+1)}^* - \epsilon(\nabla_{S_c} f(S_{c,(t+1)}^*) + B_c^T \nabla_V g(V_{(t+1)}^*))] \\
& \quad - \Pi_{\mathcal{F}}[S_{c,(t)}^* - \epsilon(\nabla_{S_c} f(S_{c,(t)}^*) + B_c^T \nabla_V g(V_{(t)}^*))]\|_2 \\
& \stackrel{b)}{\leq} \|S_{c,(t+1)}^* - \epsilon(\nabla_{S_c} f(S_{c,(t+1)}^*) + B_c^T \nabla_V g(V_{(t+1)}^*)) \\
& \quad - S_{c,(t)}^* + \epsilon(\nabla_{S_c} f(S_{c,(t)}^*) + B_c^T \nabla_V g(V_{(t)}^*))\|_2 \\
& \stackrel{c)}{\leq} \|S_{c,(t+1)}^* - \epsilon(\nabla_{S_c} f(S_{c,(t+1)}^*) \\
& \quad + B_c^T \nabla_V g(B_c S_{c,(t+1)}^* + B_l S_{l,(t)})) \\
& \quad - S_{c,(t)}^* + \epsilon(\nabla_{S_c} f(S_{c,(t)}^*) \\
& \quad + B_c^T \nabla_V g(B_c S_{c,(t)}^* + B_l S_{l,(t)}))\|_2 \\
& \quad + \|\epsilon B_c^T (\nabla_V g(B_c S_{c,(t+1)}^* + B_l S_{l,(t+1)}) \\
& \quad - \nabla_V g(B_c S_{c,(t)}^* + B_l S_{l,(t)}))\|_2 \\
& \stackrel{d)}{\leq} r(\epsilon) \|S_{c,(t+1)}^* - S_{c,(t)}^*\|_2 \\
& \quad + \epsilon\|B_c\|_2 L_g \|B_l(S_{l,(t+1)} - S_{l,(t)})\|_2 \\
& \stackrel{e)}{\leq} r(\epsilon)^k \|S_{c,(t+1)}^* - S_{c,(t)}^*\|_2 \\
& \quad + \frac{1-r(\epsilon)^k}{1-r(\epsilon)} \epsilon\|B_c\|_2 L_g \|B_l(S_{l,(t+1)} - S_{l,(t)})\|_2 \\
& \stackrel{k \rightarrow \infty}{\rightarrow} \frac{\epsilon}{1-r(\epsilon)} \|B_c\|_2 L_g \|B_l(S_{l,(t+1)} - S_{l,(t)})\|_2 \tag{27}
\end{aligned}$$

where in *a*) we use that both solutions are fixed points of the projected gradient descent (9) due to their optimality; in *b*) we remove the projection; in *c*) we use (3): $V_{(t)}^* = B_c S_{c,(t)}^* + B_l S_{l,(t)}$, we add and subtract $\epsilon B_c^T \nabla_V g(B_c S_{c,(t+1)}^* + B_l S_{l,(t)})$ and use the triangle inequality; in *d*) we use the strong convexity and the gradient Lipschitz continuity as in (23) defining $r(\epsilon) = \sqrt{1 - 2\eta\epsilon + \epsilon^2 L^2}$; in *e*) we apply the previous inequality *k* times; and in the limit we use that $|r(\epsilon)| < 1$ as explained after (24).

Since (27) is true for all ϵ such that $r(\epsilon) < 1$, we can choose $L_{S,\text{opt}} = \min_{\{r(\epsilon) < 1\}} \frac{\epsilon}{1-r(\epsilon)}$. However, note that since $\lim_{\epsilon \rightarrow 0} \frac{\epsilon}{1-r(\epsilon)} = \frac{1}{2\eta}$, the Lipschitz constant $L_{S,\text{opt}}$ is not arbitrarily small.